Desalination and Water Treatment
www.deswater.com
doi: 10.5004/dwt.2021.27233

226 (2021) 339–346
June

High-efficiency degradation of the azo dye methyl orange using Co-Mn/ZrO_2 via catalytic ozonation process

Likun Zhou[a,*], Mingming Hu[b,c], Qiang Liu[a]

[a]*CenerTech Tianjin Chemical Research and Design Institute Limited Liability Company, Tianjin 300131, China, emails: lincoln_chau@yeah.net (L. Zhou), 2849081220@qq.com (Q. Liu)*
[b]*The Institute of Seawater Desalination and Multipurpose Utilization, MNR, Tianjin 300192, China, email: 2008rosalind@gmail.com*
[c]*Tianjin Zhonghai Water Treatment Technology Co., Ltd., Tianjin 300453, China*

Received 5 August 2020; Accepted 11 March 2021

ABSTRACT

A ZrO_2 material was synthesized and optimized by the hydrothermal synthesis method with cetyltrimethylammonium bromide and $ZrOCl_2 \cdot 8H_2O$, and loaded Co and Mn bimetallic oxides to prepare the Co-Mn/ZrO_2 catalyst via an incipient wetness impregnation process. In comparison with the analogous catalyst which supported by a commercial ZrO_2, the catalyst displayed an excellent performance in the degradation of azo dye methyl orange (MO) solution via the catalytic ozonation process (COP), and the degradation efficiency of MO with 100 mg/L initial concentration would achieve 95.0% at room temperature, 1.0 mg/mL catalyst dosage, 0.65 mg/min O_3 flow, and 60 min. A series of characterizations like scanning electron microscopy, transmission electron microscopy, energy-dispersive X-ray spectroscopy, X-ray diffraction, X-ray photoelectron spectroscopy, inductively coupled plasma optical emission spectroscopy (ICP-OES) and N_2 adsorption–desorption was implemented, and showed that a larger Brunauer–Emmett–Teller reached 42.6 m^2/g and elevated the outstanding dispersion of Co and Mn oxides on ZrO_2, which accelerated the catalytic formation of hydroxyl radical from O_3 during the COP. Moreover, the Co-Mn/ZrO_2 catalyst was also investigated in the durability of catalytic MO degradation, which showed a slight diminishing trend by 6.9% for the degradation efficiency after four repetitive runs, and the loss of Co and Mn oxides from catalyst illustrated by the ICP-OES detection led to the catalyst deactivation.

Keyword: Catalytic ozonation process; Heterogeneous catalysis; Co-Mn/ZrO_2 catalyst; Dyeing wastewater; Methyl orange

1. Introduction

Because of heavy chroma, high content of organic compounds, strong toxicity and poor biodegradability, dyeing wastewater was one of the most difficult industrial sewage to be treated. It not only affected the sustainable development of the printing and dyeing industry but also posed a threat to environmental and biological health [1,2]. Azo dyes were the largest components of industrial dyes, and methyl orange (MO) was a commonly and representatively used azo dye. The conventional countermeasures for the degradation of MO contained adsorption, coagulation, Fenton oxidation, photocatalysis, biodegradation and membrane separation [3–8]. However, there were some non-competitive defects like high operating costs, inefficiency and limited environmental compatibility for all these methods above. Therefore, the catalytic ozonation process (COP) of advanced oxidation processes had been increasingly introduced for the purification of dye effluents in recent years [9].

* Corresponding author.

The COP would play an important role in generating hydroxyl radical (•OH) and degrading pollutants, and the heterogeneous catalysts such as activated carbon, metal oxides (Al_2O_3, Fe_2O_3 or MnO_2) and zeolites modified with metals [10–13] had been developed for the catalytic degradation of refractory pollutants in wastewater due to their high stability, easy separation and recycling, and non-secondary pollution. ZrO_2 was a unique transition-metal oxide that had bi-functional features of acidity and alkalinity, and the high ion-exchange capacity and redox activity made it possible to be used as a catalytic material [14]. Besides, the outstanding chemical stability and mechanical strength were favorable for the catalytic process [15], such as Fischer-Tropsch synthesis, organic reforming, photocatalysis and other fields. During to the superior oxidation ability of higher valence manganese [16], MnO_2, as an active component in heterogeneous catalyst system was widely studied, and had been proven an effective catalyst for the decomposition of some organic matters containing oxalic acid, 4-nitrophenol, pyruvic acid, sulfosalicylic and propionic acid [16–19]. MnO_2 could show high activity for O_3 decomposition in COP, for example, the MnO_2/O_3 mixed system had successfully eliminated a kind of humic and fulvic acids with 79% TOC (total organic carbon) and 89% COD (chemical oxygen demand) drop [20]. In the process of catalytic ozonation of herbicide 2,4-D, the radical scavenger tert-butanol which could capture •OH from catalysts and solution was used and availably confirmed the role of cobalt oxide supported catalyst in catalytic decomposition of O_3 into •OH, and the efficient catalysis was ascribed to the high valence oxidation state and high dispersion of cobalt oxide [21]. So, both Co and Mn high valence cations could exhibit good oxidation activities in O_3 decomposition, and the two might be the more effective components in a mixed oxides catalyst which was suitable for the redox reaction [22]. Moreover, a hybrid Co and Mn oxides active center in the form of MnO_2-Co_3O_4 nanoparticles had been reported used in the removal of benzophenone-3 under O_3 atmosphere, and the removal efficiencies increased to 64.1% and 62.6% in the MnO_2/O_3 and Co_3O_4/O_3 system, respectively, while the value was only 47.4% by O_3 alone. Nevertheless, the removal rate of benzophenone-3 enhanced to 81.2% at the same conditions over the MnO_2-Co_3O_4 further [23]. So it was worth studying the catalytic capability of catalysts loaded the two oxides of Co and Mn oxides by ZrO_2 for dye degradation with COP.

In this work, a ZrO_2 was synthesized and a related Co-Mn/ZrO_2 catalyst was prepared to promote the oxidizing capacity of O_3 on catalytic degradation of MO, and the reusability of Co-Mn/ZrO_2 was also investigated to clarify its stability. A serious characterization would help and uncover the superiority of the self-regulating catalyst in the COP.

2. Experimental

2.1. Materials and reagents

All chemicals or reagents were analytical grade and were used without any further purification. Cetyltrimethylammonium bromide (CTAB, $C_{19}H_{42}BrN$) and manganese acetate tetrahydrate ($Mn(CH_3COO)_2{\cdot}4H_2O$) were purchased from Guangfu Fine Chemical Research Institute (Tianjin, China). Zirconium oxychloride octahydrate ($ZrOCl_2{\cdot}8H_2O$) was purchased from Fucheng Chemical Reagent Co., Ltd., (Tianjin, China). Cobalt nitrate hexahydrate ($Co(NO_3)_2{\cdot}6H_2O$), ferric nitrate hydrate ($Fe(NO_3)_3{\cdot}9H_2O$), cerium nitrate hexahydrate ($Ce(NO_3)_3{\cdot}6H_2O$), sodium hydroxide (NaOH) and anhydrous ethanol were purchased from Kemiou Chemical Reagent Co., Ltd., (Tianjin, China). MO was provided by Tianjin No.1 Chemical Reagent Factory (China). And potassium iodide (KI) and the commercial ZrO_2 ($cZrO_2$) were purchased from Fengchuan Chemical Reagent Technologies Co., Ltd., (Tianjin, China) and Fanmeiya Materials Co., Ltd., (Jiangxi, China), respectively.

2.2. Instruments

The size and morphology of catalysts were characterized by scanning electron microscopy (SEM, S-4800, Hitachi, Tokyo, Japan), and transmission electron microscopy (TEM) and HAADF-STEM analyses were performed on a FEI TALOS F200 electron microscope (JEOL-2100, JEOL, Tokyo, Japan). Before SEM measurement, the catalysts were sputtered a thin layer of gold to obtain good conductivity. The phase of Co/Mn oxides loaded on ZrO_2 were characterized by an X-ray diffractometer (XRD, ULTIMA IV-J30) equipped with Cu Kα radiation (λ = 1.5418 Å). The Co and Mn valence states in catalysts were determined by X-ray photoelectron spectroscopy (XPS) on a spectrometer (ESCALAB 250Xi) performed with a monochromatic Al Kα X-ray source. During XPS measurements, the base pressure of the sample chamber was kept below 2.0×10^{-9} Mbar. The surface area and pore size distribution of materials were determined by N_2 adsorption–desorption at 77 K by Micromeritics ASAP 2420 apparatus. Before measurement, catalysts were degassed at 473 K for 24 h. The surface area and pore size distribution were obtained by Brunauer–Emmett–Teller (BET) and Barrett–Joyner–Halenda methods, respectively.

2.3. Preparation of materials

The ZrO_2 material was synthesized from $ZrOCl_2{\cdot}8H_2O$ with CTAB as the surface-active agent by the hydrothermal and calcination treatment [24]. To be specific, 16.7 g CTAB was dissolved in 83.5 mL ultrapure water with 40°C and stirred constantly for 60 min. Then, 1.5 g $ZrOCl_2{\cdot}8H_2O$ was added into the solution gradually and kept stirring for 30 min, ensuring that the Zr source dispersed evenly in CTAB. After that, NaOH (1.4 mol/L) was used to adjust the mixed solution pH value to about 11.5. All the supported catalysts concerned in this article were prepared by the incipient wetness impregnation method. For the typical catalyst of Co-Mn/ZrO_2, active component precursors of 0.37 g $Co(NO_3)_2{\cdot}6H_2O$ and 0.31 g $Mn(CH_3COO)_2{\cdot}4H_2O$ were dissolved by anhydrous ethanol with the molar ratio of Co/Mn being 1:1, then 1 g of ZrO_2 synthesized above was added into the mixed solution and stirred until the alcohol was completely evaporated at room temperature. After that, the sample was successively dried at 333 K for 2 h, dried at 383 K for 8 h, and calcined at 723 K for 2 h at air atmosphere. And in the prepared Co-Mn/ZrO_2 catalyst, the mass content of Mn element to ZrO_2 support was 7 wt.%. As a reference, the commercial $cZrO_2$ was also employed as a

support to inspect the catalytic effect of the Co-Mn/cZrO$_2$ catalyst. For comparison, the Mn/ZrO$_2$, As a promoter of catalyst, Fe or Ce is always used in the catalysts for wastewater degradation [11,12], so Fe-Mn/ZrO$_2$ and Ce-Mn/ZrO$_2$ catalysts were also prepared and employed for MO degradation. In single or double active component catalysts as mentioned above, the contents of various elements were added by the molar ratio of 1:1 to Mn, respectively.

2.4. Reaction tests

MO degradation experiments via COP were conducted in a batch reactor which was composed of a cylindrical glass reactor (1,000 mL), an O_3 generator (model NP020P-S-2, 0.65 or 1 mg/min), a glass diffuser, a flow meter, and an O_3 off-gas adsorption system (adsorbed in a 2% KI solution). Before the reaction, the MO solution (500 mL), and catalyst (0.5 g) were charged into the reactor and stirred magnetically (300 rpm).

During the reaction, the liquid-phase products were collected by an injection syringe at a certain time intervals, and then filtered with a microporous filter (0.45 μm). Before quantifying the undecomposed MO contents, the filtrates were diluted with equal amounts of ultrapure water. The degradation efficiency of MO was determined by the MO decolorization result, which was measured by the colorimetric method to test the absorbance at the maximum adsorption wavelength of 464 nm with UV-vis spectrophotometer (Genesys 10S, Thermo Fisher Scientific) , Waltham, USA, and was calculated as follows:

$$\xi = \frac{A_0 - A_t}{A_0} \times 100\% \quad (1)$$

where ξ represented the degradation efficiency of MO, A_0 and A_t was the absorbance of MO solution at 464 nm for "0" and "t" minute, respectively.

3. Results and discussion

3.1. Characterization of catalyst and support

The physical properties of the bare ZrO$_2$ or cZrO$_2$ support, fresh and used Co-Mn/ZrO$_2$ catalyst, and the cZrO$_2$ supported catalyst are summarized in Table 1. The ZrO$_2$ synthesized above had a surface area of 42.6 m^2/g, which was almost four times as much as the commercial one, accordingly, it was just the S_{BET} of cZrO$_2$ was just 13.2 m^2/g. After loaded Co and Mn oxides, the Co-Mn/ZrO$_2$ catalyst S_{BET} was 43.0 m^2/g and substantially unchanged, while the value slightly lessened to 42.2 m^2/g after being employed one time. Similarly, it was the same variation trend for pore size and volume, indicating that introduction of active components or usage would not bring about some obvious changes for the physical properties of ZrO$_2$. The Co-Mn/cZrO$_2$ catalyst also had a less surface area of only 11.1 m^2/g owning to the smaller S_{BET} of cZrO$_2$ support.

The X-ray diffraction (XRD) patterns of the ZrO$_2$ and Co-Mn/ZrO$_2$ catalyst are depicted in Fig. 1, and the diffraction peaks at 24.0°, 28.1°, 31.6°, 30.1°, 50.3° and 59.9° were attributed to the ZrO$_2$ diffraction peak. Thereinto, peaks at 24.0°, 28.1°, 31.6° belonged to the monoclinic ZrO$_2$ (m-ZrO$_2$),

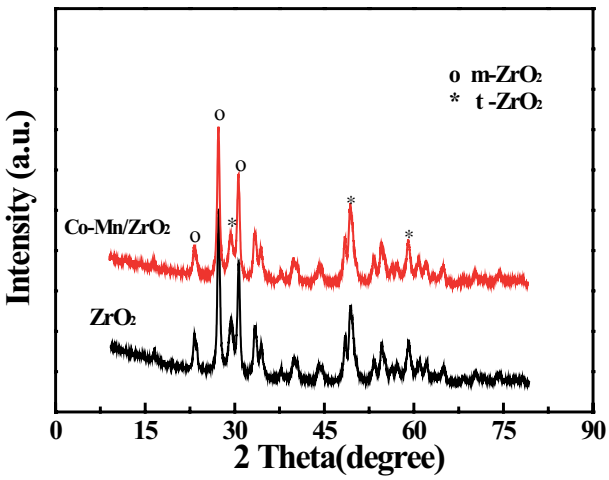

Fig. 1. XRD patterns of ZrO$_2$ support and Co-Mn/ZrO$_2$ catalyst.

and 30.1°, 50.3°, 59.9° were the peaks of tetragonal ZrO$_2$ (t-ZrO$_2$). It was believed that the prepared ZrO$_2$ mainly consisted of m-ZrO$_2$ from the peak intensity. However, being attributed to the relatively lower loading amounts of Co and Mn, and the uniform dispersion of relevant metallic oxide particles, the diffraction peaks of Co and Mn oxides were not detected from the Co-Mn/ZrO$_2$ catalyst [25,26].

The ZrO$_2$ support and Co-Mn/ZrO$_2$ catalyst were characterized by SEM, and the catalyst was further characterized by TEM, as illustrated in Fig. 2. The morphological change of ZrO$_2$ and the catalyst after loading Co and Mn oxides are shown in Figs. 2a and b. Because of the existence of metallic oxide particles on the catalyst surface, a relatively rough surface could be seen from the Co-Mn/ZrO$_2$ catalyst. Also, there was an agglomerate phenomenon on the ZrO$_2$ support, and the aggregates were about 1–3 μm. As shown in TEM image Fig. 2c, the microscopic morphology of the active ingredient of the catalyst was spherosome, elliptical spheroid or spindle shape, and the size of Co or/and Mn oxides were about 20–30 nm (Fig. 2d).

Energy-dispersive X-ray spectroscopy (EDS) microanalysis and chemical mapping of the elements were employed to reveal the distribution and relative content of various elements on the surface of ZrO$_2$. As described in Fig. 3, combining the distribution of Co, Mn, Zr and O elements with the outline of ZrO$_2$ support, it could be observed and obtained that oxides of Co and Mn were distributed uniformly on the catalyst surface. Consequently, these well-distributed active components would play an important part in the COP [23].

EDS microanalysis usually measured the relative amounts between elements on materials, and the atomic or mass fraction of loaded elements on the catalyst surface could be obtained by means of this method. The quantitative analysis results for the Co-Mn/ZrO$_2$ catalyst are summarized in Table 2. As exhibition and calculation from the atomic fraction or mass fraction, the actual molar ratio of Co/Mn was 1.09, and it was almost equivalent to the theoretical value one. Therefore, the precursors of each element dispersed evenly, Co and Mn oxides distributed uniformly, and the Co-Mn/ZrO$_2$ catalyst was well prepared.

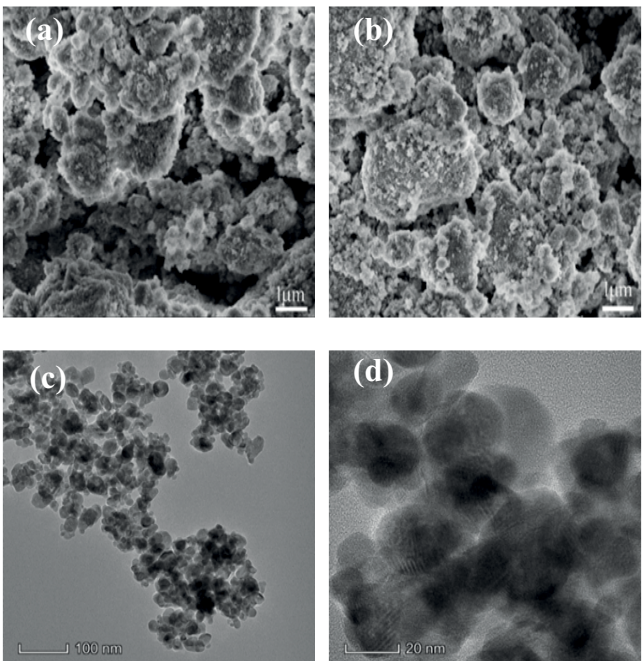

Fig. 2. SEM images of ZrO_2 (a) and Co-Mn/ZrO_2 catalyst (b), TEM images of Co-Mn/ZrO_2 catalyst (c) and (d).

To make clear the chemical states of several elements in the Co-Mn/ZrO_2 catalyst, the sample was further characterized by XPS and the spectra are shown in Fig. 4. Fig. 4a displays that Co, Mn, O and Zr elements corresponded to different peaks from the spectrum, which implied that both Co and Mn were successfully loaded on the surface of the ZrO_2. The analysis of the Co 2p spectrum in detail allowed for the assignment of the Co oxidation state. Fig. 4b depicts the XPS spectrum of Co 2p and the existence of Co was confirmed by the Co $2p_{3/2}$ peak at 781.2 eV and Co $2p_{1/2}$ peak at 796.6 eV, accompanied by shake-up satellite shoulders at 786.6 and 803.1 eV. The observed spin-orbit splitting between Co $2p_{3/2}$ and Co $2p_{1/2}$ states was at 15.4 eV. The spectral characteristic of the Co $2p_{3/2}$ peak in Fig. 4b is wide and asymmetric, which suggested the coexistence of Co(II) and Co(III), and the formation of Co_3O_4 on the surface of ZrO_2 [25,27]. Fig. 4c describes the XPS spectrum of Mn 2p, and the observed spin-orbit splitting between the two main peaks of Mn $2p_{3/2}$ and Mn $2p_{1/2}$ states was at 11.4 eV, and the binding energy of peak position of Mn $2p_{3/2}$ and Mn $2p_{1/2}$ level was at 642.1 eV and 653.5 eV, respectively. These results showed that the Mn element existed in the form of MnO_2 in the catalyst [26,28].

3.2. Catalytic performance

To illustrate the action of catalysts during MO degradation, the experiment's presence or absence of catalysts were necessary, and the degradation efficiencies of MO over a series of catalysts with or without O_3 atmosphere are intuitively compared in Fig. 5. In the absence of O_3, the removal of MO by Co-Mn/ZrO_2 catalyst was realized by its adsorption process with the removal rate was just 5.9% after 60 min. For the action of O_3 alone, only 58.2% of MO degraded at the same reaction conditions. However, the MO degradation value significantly increased with the appearance of different catalysts at O_3 atmosphere, especially with the help of Co-Mn/ZrO_2, the degradation efficiency of MO was enhanced to 95.0%. To be sure, catalysts would effectually promote MO degradation. From the degradation curve of the Co-Mn/ZrO_2 catalyst, the degradation rate descends gradually from 0 to 60 min, and the value is obviously the highest in the first 10 min. The reason might be ascribed to the increased contact chance between MO molecules and active sites of catalyst at high substrate concentration. As a contrast, the study of Co-Mn/cZrO_2 catalyst showed lower catalytic activity in COP with the degradation value of 78.1%, and the better performance of self-made ZrO_2 loaded catalyst than that of cZrO_2 should be attributed to its larger specific surface area and better distribution of active components (Table 1 and Fig. 3). About 81.2% of MO suspensions degraded over ZrO_2 support with O_3, and being impregnated and loaded Mn compounds, the Mn/ZrO_2 catalyst performance was improved slightly during the whole time of experiments. Furthermore, the Co element was introduced as an assistant composition, and the degradation ability of the Co-Mn/ZrO_2 catalyst was further improved. Consequently, it could prove that there was a synergistic effect between Mn and Co compounds [23]. In order to show the good activity of Co-Mn/ZrO_2 catalyst ulteriorly, for comparison, some other bimetallic oxides catalysts were employed for attempting to degradate MO via COP. In the Fe/Al_2O_3-SBA15 catalyst, Fe^{3+} would help the formation of •OH effectually during the catalytic ozonation, and CeO_2 could promote clofibric acid degradation and removal on Ce/MCM-48 catalyst. So Fe or Ce oxides, as an active component, were introduced to the Mn/ZrO_2. The degradation efficiency of MO over Fe-Mn/ZrO_2 or Ce-Mn/ZrO_2 catalyst was lower than that of Co-promoted catalyst through the reaction time, and the degradation values were 89.1% and 74.7%, respectively at the reaction condition of MO initial concentration 100 mg/L, catalyst dosage 1.0 mg/mL, O_3 flow 0.65 mg/min, room temperature and reaction time 60 min.

The mechanism of catalytic degradation of organic compounds by catalyst/O_3 system had been widely elaborated, and the active species was judged to be •OH which firstly generated from catalysis decomposition of O_3 by various catalysts [29,30]. •OH was a strong oxidant for its high standard electrode potential of 2.8 eV, so it was certainly very effective during the oxidative degradation processes. In previous reports, the stronger radical scavenger or indicator tert-butanol for radical type reaction was drawn into the COP to illustrate the role of catalyst. The degradation efficiency of nitrobenzene dropped more in the Mn-ceramic honeycomb and O_3 system than ozonation alone with the increase of tert-butanol concentration, so, it was easy to say that the initiation of •OH from O_3 was enhanced by the introduction of heterogeneous catalyst [29]. The catalytic ozonation of sulfamethazine under $NiCo_2O_4$ catalyst was implemented and the conclusion also clarified the •OH reaction mechanism via the COP [30]. In the quenching experiments of both single and catalytic ozonation systems, $NaHSO_3$ was used as a scavenger of •OH, and the ultimate removal results were similar. But, the removal efficiency of catalytic ozonation was more than three times that of O_3 catalysis alone in the

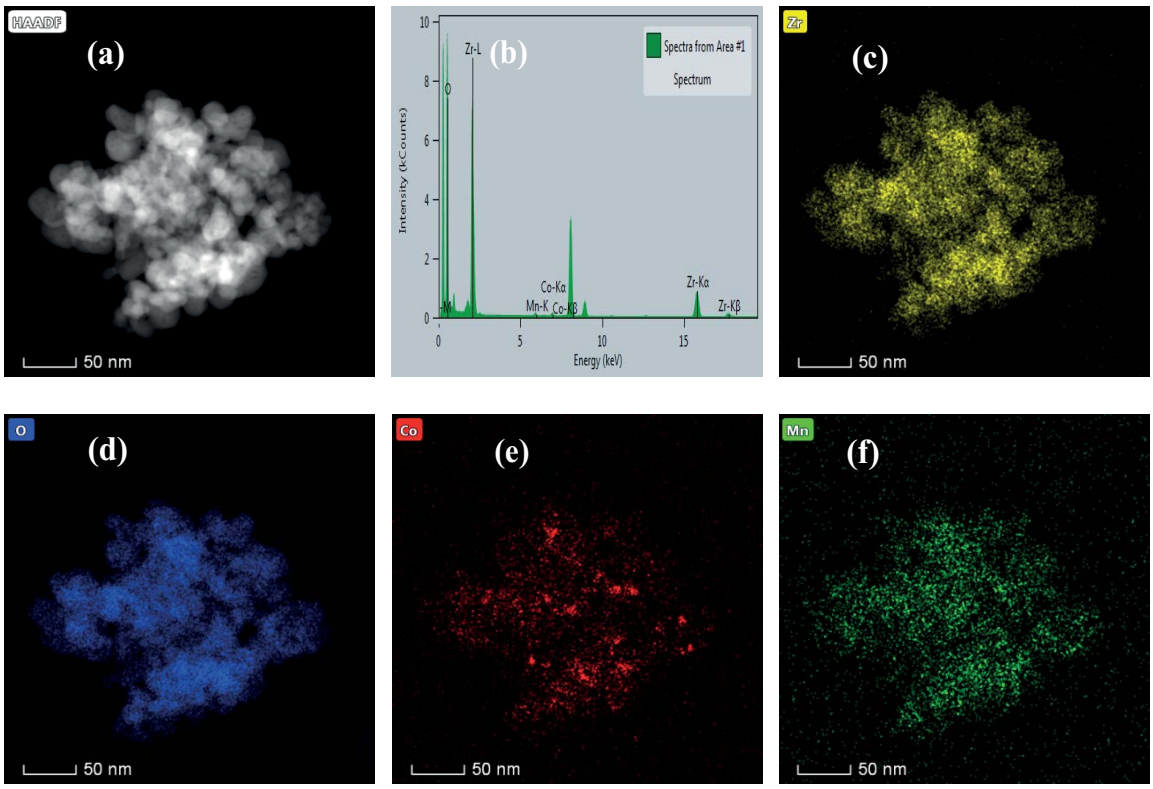

Fig. 3. Element mapping images of Co-Mn/ZrO_2 catalyst, HAADF-STEM (a), spectrum intensity (b), and the elements distribution of Zr (c), O (d), Co (e) and Mn (f).

Table 1
Physical properties of supports and catalysts

Support or catalyst	S_{BET} (m^2/g)	c (nm)	Pore volume (m^3/g)
ZrO_2	42.6	19.0	0.20
cZrO_2	13.2	20.6	0.07
Co-Mn/ZrO_2	43.0	16.5	0.18
Co-Mn/ZrO_2 (used)[a]	42.2	18.3	0.19
Co-Mn/cZrO_2	11.1	28.3	0.08

[a]catalyst was used once.

absence of $NaHSO_3$. It could be considered that the $NiCo_2O_4$ catalyst helped O_3 to decompose into more active free radicals. Obviously, the Co-Mn/ZrO_2 catalyst was the most active one among the above catalytic systems in this work, so it could indicate that Co-Mn/ZrO_2 accelerated O_3 to generate •OH which promoted the degradation of MO more efficiently. The highest catalytic activity could be ascribed to the co-existence of Co and Mn elements and a synergistic effect, or all the three parts (Co, Mn and Zr) of efforts in the catalyst [25,31]. So, it could be interpreted as more •OH generated and attacked MO molecules during the COP [32].

3.3. Catalyst stability

The stability was an important and practical index for sewage disposal catalysts, so it was necessary to investigate the cyclically catalytic efficiency of Co-Mn/ZrO_2 catalyst during COP. The catalyst was recycled four times to examine its performance for MO degradation, and the results are indicated in Fig. 6. After each run, the catalyst was filtered and washed with ultrapure water repeatedly, then dried at 120°C overnight. As expected, there was a slight reduction in the Co-Mn/ZrO_2 catalytic activity during each run. The degradation efficiency of MO reduced from 97.1% to 90.2%, that was to say, the catalyst activity cut down by 6.9% after the fourth time usage. In general, the reasons for the decrease of heterogeneous catalysts activity included active components loss and properties change for catalysts during use.

Metal ions from catalysts would lead to some negative effects, including the leaching ions could lead to a detrimental impact on the ecological security, and decrease the catalytic activity. But, the homogeneous catalytic ozonation caused by the dissolved metallic substances would make

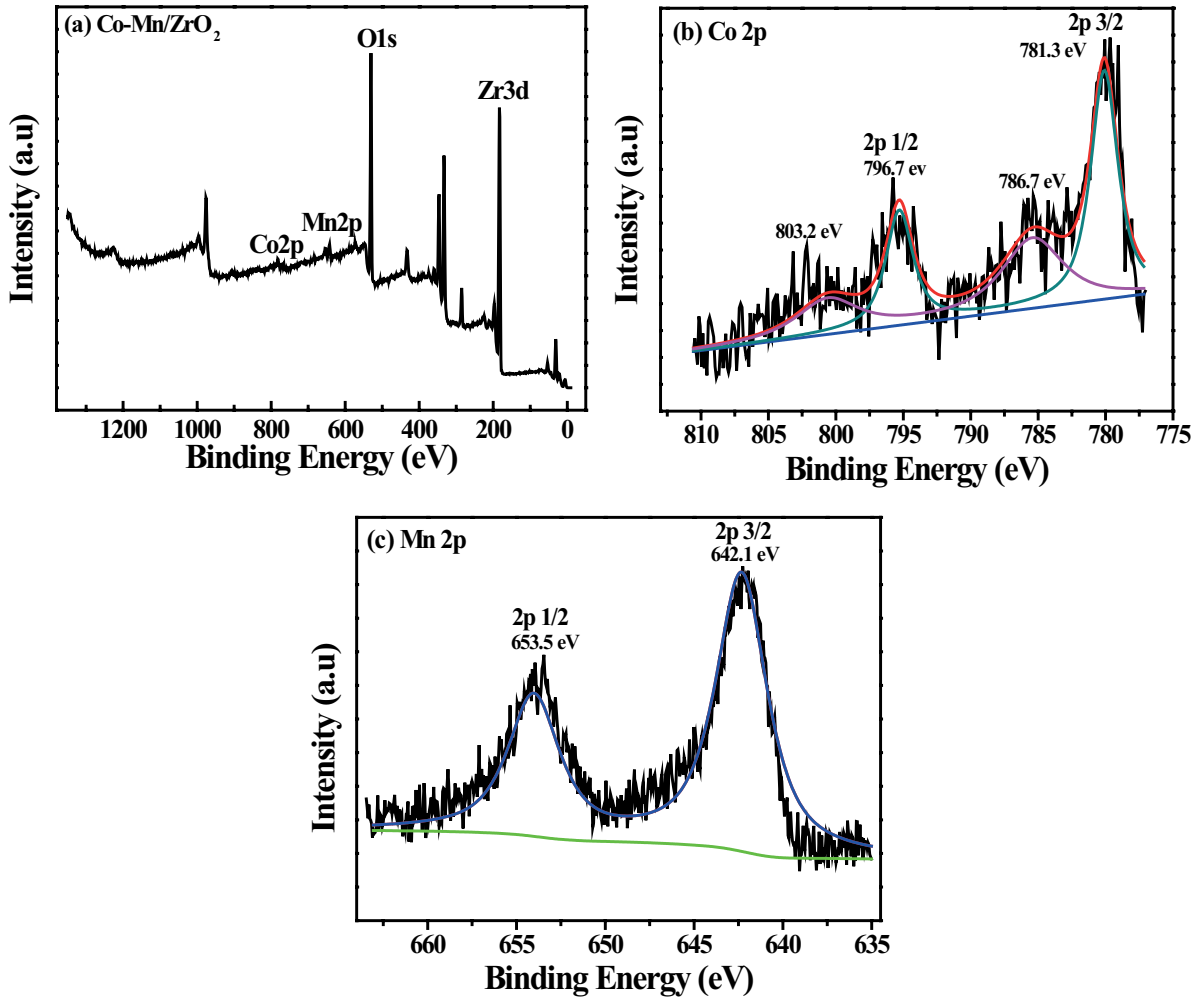

Fig. 4. XPS wide-scan spectra of Co-Mn/ZrO_2 catalyst (a), 2p XPS of Co (b) and Mn (c).

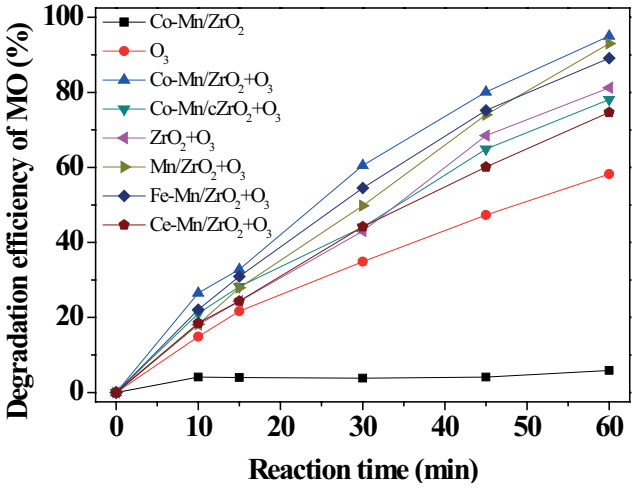

Fig. 5. Catalytic degradation of MO over different catalysts with or without O_3. (Reaction conditions: MO initial concentration 100 mg/L; catalyst dosage 1.0 mg/mL; O_3 flow 0.65 mg/min; room temperature; reaction time 60 min).

a contribution to the removal of organic compounds further [33]. Considering the above factors, it was necessary to study the leaching metal ions from COP. At the end of the first run of the Co-Mn/ZrO_2 catalyst used in MO degradation, the lost metal ions concentration in the reaction mixture was tested by inductively coupled plasma optical emission spectroscopy (ICP-OES), and the results are summarized in Table 3. It could be seen that both Co^{2+} and Mn^{2+} ions were released into the solution. The Co^{2+} and Mn^{2+} concentrations were 2.75 and 2.38 mg/L, and the loss ratio of them was 0.05% and 0.04%, respectively. The loss of Co^{2+} and Mn^{2+} could be partly responsible for the decrease in the degradation activity of the Co-Mn/ZrO_2 catalyst. In addition, although the concentration was slightly lower than the emission standards, it still needed to take some available measures to control active components leaching and improve the stability of Co-Mn/ZrO_2 catalyst more.

In addition, the change of physical or chemical properties of the catalyst in use also might cause a decrease in its activity. Due to some physical parameters like S_{BET} and pore size of Co-Mn/ZrO_2 had not varied a lot after one usage

Table 2
EDS microanalysis results of Co-Mn/ZrO_2 catalyst

Element line	Atomic fraction (%)	Mass fraction (%)
O-K	69.70	32.40
Mn-K	0.67	0.92
Co-K	0.73	1.08
Zr-K	28.90	65.60

Table 3
Leaching metal ions concentration from catalyst after the first run by ICP-OES test[a]

Leaching metal ions	Ion concentration (mg/L)	Loss ratio[a] (wt.%)
Co^{2+}	2.75	0.05
Mn^{2+}	2.38	0.04

[a]Loss ratio was mass percent content and equaled to the ratio of Co or Mn element in the solution after reaction to the corresponding element in the catalyst before employment.

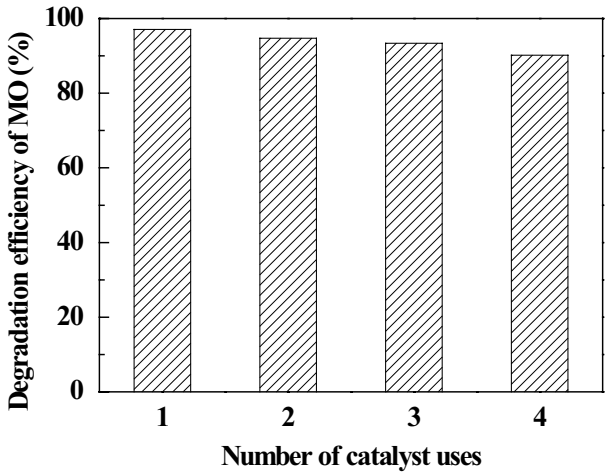

Fig. 6. Reusability of Co-Mn/ZrO_2 catalyst in MO degradation. (Reaction conditions: MO initial concentration 100 mg/L; O_3 flow 1.0 mg/min; catalyst dosage 1.0 g/L; room temperature; reaction time 60 min).

(Table 1), the side effect caused by the change of catalyst properties was predictably and mainly reflected in the following explanation. Active sites on the Co-Mn/ZrO_2 catalyst would be partially covered owing to the adsorption of organic matters from sewage by Co-Mn/ZrO_2, and the poisoning phenomenon was severe as the number of uses increasing, so the amount of $^{\bullet}OH$ species produced from O_3 in the process of interaction with catalyst would inevitably lessen too at the same Co-Mn/ZrO_2 dosage and O_3 flow.

4. Conclusions

The dependable and handy method of hydrothermal synthesis and incipient wetness impregnation was used to synthesize ZrO_2 support and prepare the Co-Mn/ZrO_2 catalyst. It exhibited an outstanding and high-efficiency catalytic performance on the degradation of MO aqueous solution via COP. It was seen that the catalytic degradation efficiency of 100 mg/L initial MO was enhanced to 95.0% with 1.0 g/L dosage of Co-Mn/ZrO_2 and 0.65 mg/min flow of O_3 at room temperature. The Co-Mn/ZrO_2 catalyst with good catalytic performance just made a relatively small decline in MO degradation through a four-times consecutive working, and a clear explanation as leaching of Co^{2+} and Mn^{2+} ions from the Co-Mn/ZrO_2 catalyst to reveal the downward trend by ICP-OES test.

Acknowledgment

This work was supported by the Science and Technology Program of Tianjin, China (18YFZCSF01440), and the Science and Technology Program of Tianjin, China (19YFZCSF01070).

References

[1] B. Okutucu, S.H. Sanlier, Decolorization of textile wastewater by dye-imprinted polymer, Desal. Water Treat., 57 (2016) 21577–21584.
[2] Y. Zhang, W.Q. Cui, W.J. An, L. Liu, Y.H. Liang, Y.F. Zhu, Combination of photoelectrocatalysis and adsorption for removal of bisphenol a over TiO_2-graphene hydrogel with 3D network structure, Appl. Catal., B, 221 (2018) 36–46.
[3] W.W. Hu, X.H. Yu, Q. Hu, J.M. Kong, L.Z. Li, X.J. Zhang, Methyl orange removal by a novel PEI-AuNPs-hemin nanocomposite, J. Environ. Sci.-China, 53 (2017) 278–283.
[4] N.M. Mahmoodi, A. Dalvand, Treatment of colored textile wastewater containing acid dye using electrocoagulation process, Desal. Water Treat., 51 (2013) 5959–5964.
[5] P. Kumar, T.T. Teng, S. Chand, K.L. Wasewar, Fenton oxidation of carpet dyeing wastewater for removal of COD and color, Desal. Water Treat., 28 (2011) 260–264.
[6] A. Sandoval, C. Hernández-Ventura, T.E. Klimova, Titanate nanotubes for removal of methylene blue dye by combined adsorption and photocatalysis, Fuel, 198 (2017) 22–30.
[7] R. Khan, P. Bhawana, M.H. Fulekar, Microbial decolorization and degradation of synthetic dyes: a review, Rev. Environ. Sci. Biotechnol., 12 (2013) 75–97.
[8] R.-R. Huang, J. Hoinkis, Q. Hu, F. Koch, Treatment of dyeing wastewater by hollow fiber membrane biological reactor, Desal. Water Treat., 11 (2009) 288–293.
[9] M.-H. Cui, D. Cui, L. Gao, A.-J. Wang, H.-Y. Cheng, Azo dye decolorization in an up-flow bioelectrochemical reactor with domestic wastewater as a cost-effective yet highly efficient electron donor source, Water Res., 105 (2016) 520–526.
[10] C.A. Orge, J.P.S. Sousa, F. Gonçalves, C. Freire, J.J.M. Órfão, M.F.R. Pereira, Development of novel mesoporous carbon materials for the catalytic ozonation of organic pollutants, Catal. Lett., 132 (2009) 1–9.
[11] J.S. Bing, C. Hu, Y.L. Nie, M. Yang, J.H. Qu, Mechanism of catalytic ozonation in Fe_2O_3/Al_2O_3@SBA-15 aqueous suspension for destruction of ibuprofen, Environ. Sci. Technol., 49 (2015) 1690–1697.
[12] S.Y. Li, Y.M. Tang, W.R. Chen, Z. Hu, X.K. Li, L.S. Li, Heterogeneous catalytic ozonation of clofibric acid using Ce/MCM-48: preparation, reaction mechanism, comparison with Ce/MCM-41, J. Colloid Interface Sci., 504 (2017) 238–246.
[13] A. Abdedayem, M. Guiza, F.J.R. Toledo, A. Ouederni, Nitrobenzene degradation in aqueous solution using ozone/cobalt supported activated carbon coupling process: a kinetic approach, Sep. Purif. Technol., 184 (2017) 308–318.
[14] X.M. Liu, G.Q. Lu, Z.F. Yan, Synthesis and stabilization of nanocrystalline zirconia with MSU mesostructure, J. Phys. Chem., B, 108 (2004) 15523–15528.

[15] M.S. Wong, D.M. Antonelli, J.Y. Ying, Synthesis and characterization of phosphated mesoporous zirconium oxide, Nanostruct. Mater., 9 (1997) 165–168.
[16] R. Andreozzi, A. Insola, V. Caprio, R. Marotta, V. Tufano, The use of manganese dioxide as a heterogeneous catalyst for oxalic acid ozonation in aqueous solution, Appl. Catal., A, 138 (1996) 75–81.
[17] F. Nawaz, H.B. Cao, Y.B. Xie, J.D. Xiao, Y. Chen, Z. Ali Ghazi, Selection of active phase of MnO_2 for catalytic ozonation of 4-nitrophenol, Chemosphere, 168 (2017) 1457–1466.
[18] R. Andreozzi, V. Caprio, A. Insola, R. Marotta, V. Tufano, The ozonation of pyruvic acid in aqueous solutions catalyzed by suspended and dissolved manganese, Water Res., 32 (1998) 1492–1496.
[19] R. Andreozzi, M.S. Lo Casale, R. Marotta, G. Pinto, A. Pollio, *N*-methyl-*p*-aminophenol (metol) ozonation in aqueous solution: kinetics, mechanism and toxicological characterization of ozonized samples, Water Res., 34 (2000) 4419–4429.
[20] M.A. Alsheyab, A.H. Muñoz, Comparative study of ozone and MnO_2/O_3 effects on the elimination of TOC and COD of raw water at the Valmayor station, Desalination, 207 (2007) 179–183.
[21] C. Hu, S.T. Xing, J.H. Qu, H. He, Catalytic ozonation of herbicide 2,4-D over cobalt oxide supported on mesoporous zirconia, J. Phys. Chem. C, 112 (2008) 5978–5983.
[22] F. Kovanda, T. Rojka, J. Dobešová, V. Machovič, P. Bezdička, L. Obalová, K. Jirátová, T. Grygar, Mixed oxides obtained from Co and Mn containing layered double hydroxides: preparation, characterization, and catalytic properties, J. Solid State Chem., 179 (2006) 812–823.
[23] Y. Guo, B.B. Xu, F. Qi, A novel ceramic membrane coated with MnO_2–Co_3O_4 nanoparticles catalytic ozonation for benzophenone-3 degradation in aqueous solution: fabrication, characterization and performance, Chem. Eng. J., 287 (2016) 381–389.
[24] J.L. Blin, R. Flamant, B.L. Su, Synthesis of nanostructured mesoporous zirconia using CTMABr-$ZrOCl_2$ center dot $8H_2O$ systems: a kinetic study of synthesis mechanism, Int. J. Inorg. Mater., 3 (2001) 959–972.
[25] S. Afzal, X. Quan, S. Chen, J. Wang, D. Muhammad, Synthesis of manganese incorporated hierarchical mesoporous silica nanosphere with fibrous morphology by facile one-pot approach for efficient catalytic ozonation, J. Hazard. Mater., 318 (2016) 308–318.
[26] H.B. Huang, X.G. Ye, W.J. Huang, J.D. Chen, Y. Xu, M.Y. Wu, Q.M. Shao, Z.R. Peng, G.C. Ou, J.X. Shi, X. Feng, Q.Y. Feng, H.L. Huang, P. Hu, D.Y.C. Leung, Ozone-catalytic oxidation of gaseous benzene over MnO_2/ZSM-5 at ambient temperature: catalytic deactivation and its suppression, Chem. Eng. J., 264 (2015) 24–31.
[27] Y.Y. Cao, C.B. Liu, J.C. Qian, Z.G. Chen, F. Chen, Novel 3D porous graphene decorated with Co_3O_4/CeO_2 for high performance supercapacitor power cell, J. Rare Earths, 35 (2017) 995–1001.
[28] D.A. Aguilera, A. Perez, R. Molina, S. Moreno, Cu–Mn and Co–Mn catalysts synthesized from hydrotalcites and their use in the oxidation of VOCs, Appl. Catal., B, 104 (2011) 144–150.
[29] L. Zhao, J. Ma, Z.-Z. Sun, X-.D. Zhai, Catalytic ozonation for the degradation of nitrobenzene in aqueous solution by ceramic honeycomb-supported manganese, Appl. Catal., B, 83 (2008) 256–264.
[30] H. Chen, J.L. Wang, Catalytic ozonation for degradation of sulfamethazine using $NiCo_2O_4$ as catalyst, Chemosphere, 268 (2020) 128840–128850.
[31] F. Li, Y.C. Dong, W.M. Kang, B.W. Cheng, G.X. Cui, Enhanced removal of azo dye using modified PAN nanofibrous membrane Fe complexes with adsorption/visible-driven photocatalysis bifunctional roles, Appl. Surf. Sci., 404 (2017) 206–215.
[32] R. Kumar, G. Kumar, A. Umar, ZnO nano-mushrooms for photocatalytic degradation of methyl orange, Mater. Lett., 97 (2013) 100–103.
[33] H.N. Li, B.B. Xu, F. Qi, D.Z. Sun, Z.L. Chen, Degradation of bezafibrate in wastewater by catalytic ozonation with cobalt doped red mud: efficiency, intermediates and toxicity, Appl. Catal., B, 152–153 (2014) 342–351.